J. Fluid Mech. (1993), *vol.* 250, *pp.* 103–119

Excitation of capillary waves by longer waves

By KENNETH M. WATSON[1] AND JOHN B. McBRIDE[2]

[1] Marine Physical Laboratory, Scripps Institution of Oceanography, University of California at San Diego, San Diego, CA 92093-0213, USA

[2] Science Applications International Corporation, 10260 Campus Point Drive, San Diego, CA 92121, USA

(Received 26 May 1992 and in revised form 19 October 1992)

At low wind speeds the shortest capillary waves appear to be generated hydrodynamically and not by the wind. This phenomenon is investigated using a Hamiltonian representation of the surface wave dynamics. A perturbation technique of Kolmogorov is used to transform away non-resonant, nonlinear interactions. Resonant interactions are treated by the Hasselmann transport equation, applied to the transformed variables. Calculated spectra show reasonable agreement with the observations of Jähne & Riemer (1990).

1. Introduction

In a recent series of experiments Jähne & Riemer (1990) have studied the spectrum of short gravity–capillary waves for wavelengths in the range $0.4 < \lambda < 24$ cm. These experiments were performed in a large tank at a fetch of 100 m and with wind speeds (U) from 3 to 17 m/s. An important conclusion of these observations is that at low wind speeds generation of capillary waves by longer waves is a significant mechanism for determining the capillary spectrum. A second conclusion from the Jähne–Riemer (1990) observations is that the capillary spectrum cuts off below a wavelength λ of about 0.6 cm, even at high wind speeds. Some related conclusions concerning the generation of short capillary waves have been reported by Cox (1958) and Miller, Shemdin & Longuet-Higgins (1992). An early theoretical treatment of capillary wave generation by longer waves was given by Longuet-Higgins (1962).

As noted by Jähne & Riemer (1990), their observations show a difficulty for spectral models, such as that of Donelan & Pierson (1987), which employ a local balance in wavenumber space between energy input and dissipation. For example, with a growth rate due to wind $\beta_w(\boldsymbol{k})$ and a dissipation rate due to viscosity $\beta_v(\boldsymbol{k})$ at wavenumber $\boldsymbol{k}$, the Donelan–Pierson spectrum (we refer to this as the D-P spectrum) $\Psi(\boldsymbol{k})$ vanishes for $\boldsymbol{k}$ such that $\beta_v > \beta_w$. The spectra observed by Jähne & Riemer extend beyond this range. This is illustrated in figure 1, where we show the dimensionless D-P spectrum $B(\boldsymbol{k})$ (defined by (2.45)) for a wind speed U (at 10 m elevation) of 5 m/s. This spectrum vanishes for $\lambda < 1$ cm. We have indicated two regimes in this figure: the 'wind-generated regime' and the 'dynamically generated regime', where the D-P spectrum vanishes.

This shortcoming of theories which assume a local balance in wavenumber space ($\boldsymbol{k}$-space) is well recognized. The equations of fluid mechanics imply nonlinear flow of energy through $\boldsymbol{k}$-space and the transport theory of Hasselmann (1968) for weakly nonlinear waves provides a model for this.

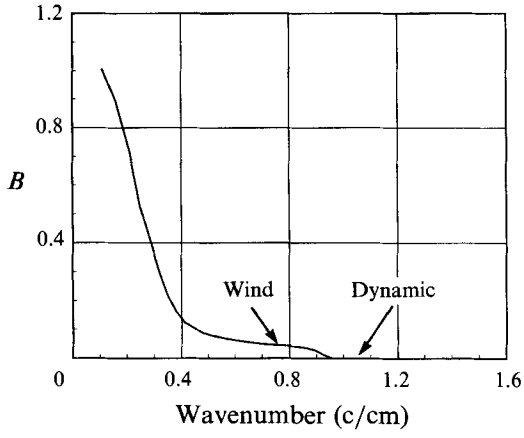

FIGURE 1. The dimensionless Donelan–Pierson surface wave spectrum is shown for a wind speed of 5 m/s and waves travelling downwind. The 'wind' region is that for which the D-P spectrum is non-vanishing. The 'dynamic' region is that beyond the cutoff, where capillary waves are generated by longer waves.

Models to describe the evolution of the surface wave spectrum are often written in the form

$$\frac{\partial F(\boldsymbol{k})}{\partial t} = S_{\mathrm{nl}} + S_{\mathrm{w}} + S_{\mathrm{v}}. \tag{1.1}$$

Here $F(\boldsymbol{k})$ is the wave action density at wavenumber $\boldsymbol{k}$. The effects of wind and viscous damping are represented, respectively, by the terms S_{w} and S_{v}. Other effects, such as nonlinear interactions, are expressed by S_{nl}. Theoretical models for S_{nl} have been obtained using, for example, the Hasselmann (1968) technique. Phenomenological models have been proposed by Hughes (1978), Phillips (1985), and D-P. Since most studies have concentrated on gravity waves and our interest here is in capillary waves, we shall write

$$S_{\mathrm{nl}} = S_{\mathrm{t}} + S_{\mathrm{DP}}, \tag{1.2}$$

where S_{t} describes capillary–gravity wave interactions and S_{DP} represents the remainder of S_{nl}. We have used the subscript 'DP' here in anticipation of later use of the D-P model.

At this point we give a schematic description of our model for calculating the capillary wave spectrum. The detailed implementation for this is given in §3. We write

$$F(\boldsymbol{k}) = F_{\mathrm{D}}(\boldsymbol{k}) + F_{\mathrm{c}}(\boldsymbol{k}), \tag{1.3}$$

where F_{D} satisfies the equation

$$\frac{\partial F_{\mathrm{D}}(\boldsymbol{k})}{\partial t} = S_{\mathrm{DP}} + S_{\mathrm{w}} + S_{\mathrm{v}} = 0 \tag{1.4}$$

in which we have set $F_{\mathrm{c}} = 0$. The quantity F_{D} obtained from (1.4) represents an equilibrium spectrum in the absence of capillary wave interactions. The term F_{c} in (1.3) describes the modification of the spectrum due to capillary wave interactions. Equations (1.1) and (1.4) suggest the equilibrium model

$$\frac{\partial F_{\mathrm{c}}(\boldsymbol{k})}{\partial t} = S_{\mathrm{t}} = 0, \tag{1.5}$$

where the quantity F_D obtained from (1.4) is used to evaluate S_t. We shall call this the 'direct-generation' model.

An alternative model is obtained directly from (1.1):

$$S_t + S_{DP} + S_w + S_v = 0. \tag{1.6}$$

Here F is evaluated without using the decomposition (1.3). Specifically, the term F_c is now included in S_{DP} in (1.6). We shall refer to this as the 'modified D-P' model. Evidently, both of these models involve some judgement in the mix of phenomenology and theory. The direct-generation model involves less empiricism, while the modified D-P model includes more physical detail. We shall find that because of the strength of the nonlinear interactions, these two models yield similar spectra.

Calculations of the interaction of capillary waves with capillary/gravity waves have been published by Valenzuela & Laing (1972), Holliday (1977), and van Gastel (1987*a*, *b*). These calculations, which use the Hasselmann (1968) theory to calculate S_t, include only the lowest-order nonlinear interactions (terms of second order in the mode amplitude equations), for which three-wave resonances are encountered with capillary waves. For purely gravity waves, the lowest-order resonances are four-wave resonances arising from terms of third order in the equations of motion. To the extent that the wave–wave interactions are 'weakly nonlinear' it has appeared reasonable in the above work to truncate the equations for capillary waves at second order, keeping only three-wave resonant effects.

An approach that is complementary to that of the Hasselmann theory was adopted by Creamer *et al.* (1989), who use the Hamiltonian formulation for surface wave dynamics. They consider only gravity waves (so three-wave resonances do not occur) and truncate the Hamiltonian above third order in the wave amplitudes. Without resonances, they can employ conventional canonical transformation theory to obtain new variables for which there are no nonlinear interactions (to the truncated order). These 'quasi-linear' waves satisfy the usual linear wave dispersion relation. Creamer *et al.* (1989, referred to herein as CHSW) argue that it is these quasi-linear wave amplitudes that should be considered as having the properties of a random Gaussian field. Inverse transformation back to the physical variables gives the 'physical waves'. Effects of straining, advection, and vertical acceleration were obtained by this procedure, which includes WKB-like phenomena in long wave–short wave interactions (see Henyey *et al.* 1988, for a related discussion). A surprisingly realistic sea surface image with sharp-crested waves was obtained by CHSW. Also, this method gave a good representation of a Stokes wave.

The canonical transformation theory fails to deal with resonances.† Thus, the transformation theory of CHSW cannot give any account of resonant effects in wave–wave interactions. At the same time, the Hasselmann transport theory fails to describe phase-coherent coupling of waves having different wavelengths, effects that were demonstrated by CHSW. The cummulant discard approximation used in deriving the Hasselmann equation is at fault here.

In this paper we attempt to merge the Hasselmann technique with that of the canonical transformation theory, following a suggestion of Meiss & Watson (1978). They proposed applying the canonical transformation theory only in the domain where there are no resonant interactions. All non-resonant interactions were to be removed to a prescribed nonlinear order using the 'superconvergent' perturbation theory of Kolmogorov (see Chirikov 1977). The resulting 'quasi-linear' waves would be linear,

† An excellent review of this and other aspects of the Hamiltonian description for many-dimensional nonlinear oscillators has been given by Chirikov (1977).

except for the resonances. Hasselmann theory or numerical integration, for example, could be used to treat the resonant wave interactions. The final step would be the inverse transformation back to physical variables. The physical consequence is that the Hasselmann technique is augmented with phase-coherent long wave–short wave couplings.

In §3 we carry out the prescriptions implied by (1.4) and (1.5) and by (1.6) for 'quasi-linear' waves. The CHSW transformation back to 'physical waves' is done in §4 to yield the physical wave spectra.

A transformation theory similar to that of CHSW was used by Watson & West (1975), who employed a perturbuation approach suggested by that of Krylov and Bogoliubov (see Case 1966). This method works directly from the equations of motion and does not use a Hamiltonian representation. Effects of external energy sources and dissipation may then be readily included. We prefer here the use of a Hamiltonian because of its greater simplicity and because in the wavelength and wind regime of principal interest to us the nonlinear interactions tend to be more important than are the effects of wind or viscosity.

Following the implications of the Jähne & Riemer (1990) observations, we shall assume that there are no waves having wavelengths less than 0.6 cm. We are interested in the capillary wave spectrum for low wind speeds ($U \leqslant 6$ m/s) and at wavelengths near the vanishing point of the D-P spectrum and in the 'dynamic' range of figure 1.

2. Quasi-linear waves

We assume inviscid, irrotational flow with a velocity potential $\Phi(\boldsymbol{x}, z)$. We take the reference plane at $z = 0$ to be that of the local undisturbed water surface and $\boldsymbol{x} = (x, y)$ to be a vector in that plane. The vertical displacement of the water surface from the reference plane at location $\boldsymbol{x}$ is $\zeta(\boldsymbol{x})$. The velocity potential at the water surface is then

$$\phi(\boldsymbol{x}) = \Phi(\boldsymbol{x}, \zeta(\boldsymbol{x})). \tag{2.1}$$

The fluid equations for surface waves may be written in Hamiltonian form (Miles 1977; West 1981; Milder 1990) using these variables. We refer to Milder (1990) for details and shall follow his notation.

The vertical component of fluid velocity w at the surface is expressed in terms of a non-local operator $\hat{\mathbf{D}}$,

$$w = \left.\frac{\partial \Phi}{\partial z}\right|_{z=\zeta} \equiv \hat{\mathbf{D}}\phi. \tag{2.2}$$

The horizontal component of fluid velocity at the surface is

$$\boldsymbol{u} = \boldsymbol{\nabla}\Phi_{z=\zeta} \equiv \boldsymbol{\nabla}_{\mathrm{h}}\phi \equiv \boldsymbol{\nabla}\phi - w\boldsymbol{\nabla}\zeta, \tag{2.3}$$

defining the operator $\boldsymbol{\nabla}_{\mathrm{h}}$. The operator $\boldsymbol{\nabla}$ here is the gradient operator acting in the (x, y)-plane.

Using the notation of Milder (1990) and normalizing energy and action to unit water density, the Hamiltonian, which is also the energy of the wave system, is

$$H = \frac{1}{2}\int [\phi\hat{\mathbf{K}}\phi + g\zeta^2 + 2\tau(1 + (\boldsymbol{\nabla}\zeta)^2)^{\frac{1}{2}} - 2\tau]\,\mathrm{d}\boldsymbol{x}. \tag{2.4}$$

Here g is the acceleration due to gravity,

$$\tau \approx 7.5 \times 10^{-5}\ \mathrm{m}^3/\mathrm{s}^2 \tag{2.5}$$

represents a nominal value for surface tension, and $\hat{\mathrm{K}}$ is the operator

$$\hat{\mathrm{K}} = [1+(\nabla\zeta)^2]\hat{\mathrm{D}} - \nabla\zeta\cdot\nabla. \tag{2.6}$$

The equations of motion are

$$\frac{\partial\zeta}{\partial t} = \frac{\delta H}{\delta\phi}, \quad \frac{\partial\phi}{\partial t} = -\frac{\delta H}{\delta\zeta}. \tag{2.7}$$

Milder (1990) discusses in some detail means for practical use of the operators $\hat{\mathrm{D}}$ and $\hat{\mathrm{K}}$.

We now introduce a Fourier representation† in a larger rectangular area A_0

$$\left.\begin{aligned} \phi(\boldsymbol{x}) &= \sum_{k}[V_k/(2A_0)]^{\frac{1}{2}}[a_k\,\mathrm{e}^{\mathrm{i}k\cdot x}+\mathrm{c.c.}], \\ \zeta(\boldsymbol{x}) &= \mathrm{i}\sum_{k}[1/(2A_0\,V_k)^{\frac{1}{2}}][a_k\,\mathrm{e}^{\mathrm{i}k\cdot x}-\mathrm{c.c.}]. \end{aligned}\right\} \tag{2.8}$$

Here

$$V_k = \omega_k/k \tag{2.9}$$

is the linear wave phase velocity and

$$\omega_k = [k(g+\tau k^2)]^{\frac{1}{2}} \tag{2.10}$$

is the liner wave angular frequency. The Fourier amplitudes a_k are 'action amplitudes', expressed in terms of canonical action-angle variables J_k and θ_k as

$$a_k = J_k^{\frac{1}{2}}\,\mathrm{e}^{-\mathrm{i}\theta_k}. \tag{2.11}$$

The Poisson bracket relations for the a_k are

$$\left.\begin{aligned} \{a_k, a_{k'}\} &\equiv \sum_{p}\left[\frac{\partial a_k}{\partial\theta_p}\frac{\partial a_{k'}}{\partial J_p}-\frac{\partial a_k}{\partial J_p}\frac{\partial a_{k'}}{\partial\theta_p}\right] = 0, \\ \{a_k, a_{k'}^*\} &= -\delta_{k-k'}, \end{aligned}\right\} \tag{2.12}$$

where δ_k is the discrete δ-function. Equations of motion for the amplitudes a_k are

$$\dot{a}_k = \{a_k, H\}. \tag{2.13}$$

The equations to determine the action-angle variables are

$$\dot{J}_k = \{J_k, H\} = -\partial H/\partial\theta_k, \qquad \dot{\theta}_k = \{\theta_k, H\} = \partial H/\partial J_k. \tag{2.14}$$

We expect the energy to increase with increasing action. Thus, $\dot{\theta}_k > 0$ and we see from (2.8) and (2.11) that a_k represents the amplitude of a wave propagating in the direction of $\boldsymbol{k}$.

The spectrum of vertical displacement is seen from (2.8) to be

$$\Psi(\boldsymbol{k}) = \langle|a_k|^2\rangle/[(2\pi)^2\,V_k], \qquad \langle\zeta^2\rangle = \int \mathrm{d}\boldsymbol{k}\,\Psi(\boldsymbol{k}). \tag{2.15}$$

Here the angle brackets represent an ensemble average over many realizations of the wave system. The action density of the linear system is

$$F(\boldsymbol{k}) = V_k\,\Psi(\boldsymbol{k}), \tag{2.16}$$

† See Watson & West (1975) for more detail. The Fourier expansion is made on their variable $Z(\boldsymbol{x}, t)$ in terms of which ϕ and ζ are expressed.

or, equivalently,

$$\sum_k J_k/A_0 = \int \mathrm{d}\boldsymbol{k}\, F(\boldsymbol{k}). \tag{2.17}$$

Milder (1990) describes the expansion of (2.4) in ascending orders of the field variables. He obtains

$$H(J,\theta) = H_0(J) + \epsilon H_1(J,\theta) + \epsilon^2 H_2(J,\theta) + \ldots, \tag{2.18}$$

where ϵ is a formal expansion parameter that will later be set equal to unity and

$$H_0 = \frac{1}{2}\int [\phi \hat{\mathrm{k}}\phi + g\zeta^2 + \tau(\nabla\zeta)^2]\,\mathrm{d}\boldsymbol{x}, \tag{2.19}$$

$$H_1 = \frac{1}{2}\int \zeta[(\nabla\phi)^2 - (\hat{\mathrm{k}}\phi)^2]\,\mathrm{d}\boldsymbol{x}, \tag{2.20}$$

$$H_2 = -\frac{1}{4}\int \{(\hat{\mathrm{k}}\phi[\zeta,[\zeta,\hat{\mathrm{k}}]]\,\hat{\mathrm{k}}\phi + \tfrac{1}{2}\tau(\nabla\phi)^4\}\,\mathrm{d}\boldsymbol{x}. \tag{2.21}$$

In these expressions $\hat{\mathrm{k}}$ is the operator defined as

$$\hat{\mathrm{k}}^2 = -\nabla^2. \tag{2.22}$$

Thus,

$$\hat{\mathrm{k}}\,\mathrm{e}^{\mathrm{i}\boldsymbol{p}\cdot\boldsymbol{x}} = p\,\mathrm{e}^{\mathrm{i}\boldsymbol{p}\cdot\boldsymbol{x}}, \tag{2.23}$$

The commutator symbol $[A,B] = AB\text{-}BA$ is used in (2.21).

On introducing the Fourier expansions (2.8) into (2.19) and (2.20) we obtain

$$H_0 = \sum_k \omega_k J_k, \tag{2.24}$$

$$H_1 = -\sum_{k,l,m}\left(\frac{J_k J_l J_m}{8A_0}\right)^{\frac{1}{2}}\left\{\delta_{k+l+m}\left(\frac{V_l V_m}{V_k}\right)^{\frac{1}{2}}(\boldsymbol{l}\cdot\boldsymbol{m} + lm)\sin(\theta_k+\theta_l+\theta_m)\right.$$
$$\left. + \delta_{k-l-m}\frac{\Gamma(\boldsymbol{k},\boldsymbol{l},\boldsymbol{m})}{(V_k V_l V_m)^{\frac{1}{2}}}\sin(\theta_k-\theta_l-\theta_m)\right\}. \tag{2.25}$$

here Γ is the expression introduced by van Gastel (1987*a*):

$$\Gamma(\boldsymbol{k},\boldsymbol{l},\boldsymbol{m}) = \omega_k\omega_l(\hat{\boldsymbol{l}}\cdot\hat{\boldsymbol{k}} - 1) + \omega_k\omega_m(\hat{\boldsymbol{m}}\cdot\hat{\boldsymbol{k}} - 1) + \omega_l\omega_m(\hat{\boldsymbol{l}}\cdot\hat{\boldsymbol{m}} + 1). \tag{2.26}$$

A similar expansion in terms of four interacting waves may be given for H_2. With a minor exception, we do not need H_2 and shall truncate our equations beyond the first power of ϵ. We will therefore not show the rather long expression for H_2.

Our next objective is to transform away as much of H_1 as we can with a canonical transformation to new action-angle variables I_k, ϕ_k. The amplitudes of these 'quasi-linear' waves will then be of the form (2.11)

$$A_k = I_k^{\frac{1}{2}}\mathrm{e}^{-\mathrm{i}\phi_k}. \tag{2.27}$$

We shall consider these amplitudes to be Gaussian, as was proposed by CHSW. The Hamiltonian expressed in these new variables is then

$$K(I,\phi) = H(J,\theta). \tag{2.28}$$

A general discussion of canonical transformation theory is given, for example, by Goldstein (1959). We shall use the Lie method as used in CHSW, adapted to the

'superconvergent' perturbation theory of Kolmogorov (see Chirikov, 1977). Meiss & Watson (1978) describe the application of this perturbation theory to obtain 'quasi-linear' waves.

Following CHSW we introduce canonical variables $Q_i(\lambda), P_i(\lambda)$ as functions of a parameter λ defined in the interval $0 \leqslant \lambda \leqslant 1$. Limiting values of these variable are

$$Q_i(0) = \theta_i, \quad P_i(0) = J_i; \qquad Q_i(1) = \phi_i, \quad P_i(1) = I_i. \tag{2.29}$$

The variables Q, P are determined from a generating function R:

$$\partial Q_i/\partial\lambda = \{Q_i, R\}, \quad \partial P_i/\partial\lambda = \{P_i, R\}. \tag{2.30}$$

These relations may be re-expressed as integral equations, as was done in CHSW,

$$Q_i(\lambda) = \phi_i - \epsilon\int_\lambda^1 \mathrm{d}\lambda'\{Q_i(\lambda'), R(\lambda')\}, \quad P_i(\lambda) = I_i - \epsilon\int_\lambda^1 \mathrm{d}\lambda'\{P_i(\lambda'), R(\lambda')\}. \tag{2.31}$$

The relation between the original and the new variables is then

$$\theta_i = \phi_i - \epsilon\int_0^1 \mathrm{d}\lambda'\{Q_i, R\} \equiv \phi_i - \epsilon\,\Delta\phi_i, \quad J_i = I_i - \epsilon\int_0^1 \mathrm{d}\lambda'\{P_i, R\} \equiv I_i - \epsilon\Delta I_i. \tag{2.32}$$

The next step in applying the superconvergent perturbation theory is the substitution

$$K_1(I,\theta) = H(I-\epsilon\Delta I,\theta) = H_0(I) - \epsilon\sum_j \frac{\partial H_0}{\partial I_j}\Delta I_j + \epsilon H_1(I,\theta) - \epsilon^2\sum_j \frac{\partial H_1}{\partial I_j}\Delta I_J + \epsilon^2 H_2(I,\theta) + O(\epsilon^3). \tag{2.33}$$

We now split H_1 into 'resonant' and 'non-resonant' parts:

$$H_1 = H_{1\mathrm{N}} + H_{1\mathrm{R}} \tag{2.34}$$

and eliminate the non-resonant part $H_{1\mathrm{N}}$ by setting

$$\sum_j \omega_j \Delta I_j = H_{1\mathrm{N}}(I,\theta). \tag{2.35}$$

Here we have used (2.24) to write

$$\partial H_0/\partial I_j = \omega_j.$$

We are left with

$$K_1(I,\theta) = H_0(I) + \epsilon H_{1\mathrm{R}}(I,\theta) + \epsilon^2 H_{2\mathrm{T}} + O(\epsilon^3), \tag{2.36}$$

where

$$H_{2\mathrm{T}}(I,\theta) \equiv H_2(I,\theta) - \sum_j \frac{\partial H_1}{\partial I_j}\Delta I_j. \tag{2.37}$$

The next step of the superconvergent theory is an average over the angles θ in (2.33). For a function $f(I,\theta)$ we use the notation

$$f(I,\theta) = \bar{f}(I) + \tilde{f}(I,\theta),$$

where $\bar{f}(I)$ is the value of f after averaging over all θ. We note that $\bar{H}_{1\mathrm{R}} = 0$, so can rewrite (2.33) as

$$K_1(I,\theta) = K_0(I) + \epsilon H_{1\mathrm{R}}(I,\theta) + \epsilon^2\tilde{H}_{2\mathrm{T}} + O(\epsilon^3), \tag{2.38}$$

where

$$K_0(I) = H_0(I) + \epsilon^2\bar{H}_{2\mathrm{T}}(I). \tag{2.39}$$

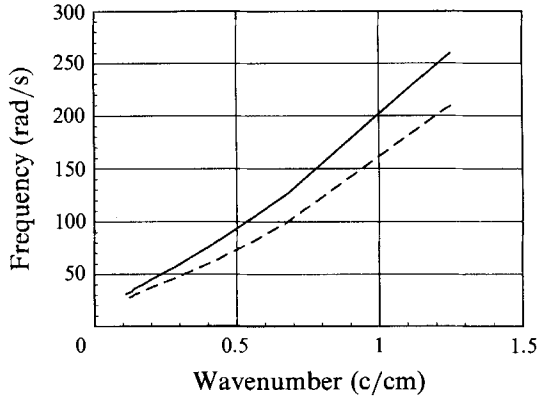

FIGURE 2. The 'dressed wave' frequency determined from (2.40) (solid curve) is compared with the linear wave frequency (dashed curve). Here the wind speed is taken to be 6 m/s and the waves are travelling downwind.

A nonlinear frequency shift is exhibited by the θ-average:

$$\dot{\phi}_j \equiv \Omega_j = \frac{\partial K_0}{\partial I_j} \equiv \omega_j + \epsilon^2 \Delta\Omega_j + \ldots. \tag{2.40}$$

The final transformed Hamiltonian (2.28) is

$$K(I,\phi) = K_1(I, \phi - \epsilon\Delta\phi) = K_0(I) + \epsilon H_{1R}(I,\phi) + O(\epsilon^2). \tag{2.41}$$

To satisfy (2.35) we follow the prescription of CHSW, where more detail is given. The integral equations (2.31) may be iterated to develop a power series in ϵ. We require only the lowest order, which gives

$$\Delta\phi_i \approx \partial R/\partial I_i, \quad \Delta I_i \approx -\partial R/\partial\phi_i. \tag{2.42}$$

The transformation function R, which satisfies (2.35), is in our notation

$$R(I,\phi) = -\sum_{k,l,m} \frac{(I_k I_l I_m)^{\frac{1}{2}}}{2(2A_0)^{\frac{1}{2}}} \left\{ \delta_{k+l+m} \left(\frac{V_l V_m}{V_k} \right)^{\frac{1}{2}} \frac{\boldsymbol{l}\cdot\boldsymbol{m} + lm}{\omega_k + \omega_l + \omega_m} \cos(\theta_k + \theta_l + \theta_m) \right.$$
$$\left. + \delta_{k-l-m} \frac{\Gamma(\boldsymbol{k},\boldsymbol{l},\boldsymbol{m})}{\omega_k - \omega_l - \omega_m} \frac{\cos(\theta_k - \theta_l - \theta_m)}{(V_k V_l V_m)^{\frac{1}{2}}} \right\}. \tag{2.43}$$

We emphasize that the domain of triad resonances is omitted from the sums in (2.43), as will be described in more detail below.

The significance of the phase averaging, as in (2.38), is that the frequency shift $\Delta\Omega_k$ in (2.40) leads to a phase shift in the ϕ_k that grows indefinitely with time. If we assume that $k \gg 1$, a straightforward but tedious calculation gives (after a welcome sequence of cancellations of 'larger' terms proportional to k^2 *and* $k^{\frac{3}{2}}$)

$$\Omega_k = \omega_k + 2\boldsymbol{k} \cdot \int \mathrm{d}\boldsymbol{l}\, \Psi(\boldsymbol{l})\, \omega_l\, \boldsymbol{l}[1 + O(l/k)^{\frac{1}{2}}]. \tag{2.44}$$

This same result, which describes advection by drift currents of the longer waves, was obtained by Watson & West (1975)†.

The frequency (2.40) is compared with linear wave frequency in figure 2. In evaluating this we used the composite D-P spectrum, which specifies the spectrum of

† The coefficient 2 in (2.44) was given as 7/2 in the Watson–West paper. This was presumably an arithmetic error since the formal expressions for the frequency shift there is the same as that obtained here.

Donelan, Hamilton & Hui (1985) at longer wavelengths. The wind speed at 10 m elevation is assumed to be 6 m/s. The shift from the linear frequency, as given by (2.44), agrees to within about 25% with that obtained from (2.40). The frequency shift (2.40) can shift the triad resonance conditions; however, the approximate shift (2.44) will not do this. Since the frequency shifts are relatively small and since the expressions (2.40) and (2.44) are in fair agreement, we shall here use the linear frequencies in evaluating the triad resonance conditions.

The relatively slowly varying dimensionless spectrum $B(\boldsymbol{l})$, called the 'degree of saturation' by Phillips (1985), is more convenient than $\Psi(\boldsymbol{l})$ to use for analysis of broad spectral bands. This quantity is defined by the equation

$$\Psi(\boldsymbol{l}) = \alpha_{\mathrm{D}} B(\boldsymbol{l})/l^4, \tag{2.45}$$

where

$$\alpha_{\mathrm{D}} = 4\times 10^{-3} \tag{2.46}$$

is a dimensionless parameter.

3. The spectral transport equation

The quasi-linear amplitudes (2.27) satisfy the equations of motion

$$\dot{A}_k = \{A_k, K\}. \tag{3.1}$$

Evaluation of (3.1) using (2.25), (2.27), and (2.41) leads to the coupled equation

$$\dot{A}_k + \mathrm{i}\Omega_k A_k = \sum_{l,p} \frac{1}{4(2A_0)^{\frac{1}{2}}} \{[\delta_{k-l-p}\Gamma(\boldsymbol{k},\boldsymbol{p},\boldsymbol{l})\, A_l A_p - 2\delta_{k-l+p}\Gamma(\boldsymbol{l},\boldsymbol{k},\boldsymbol{p})\, A_l A_p^*]/(V_k V_l V_p)^{\frac{1}{2}} + \delta_{k+l+p} h(\boldsymbol{l},\boldsymbol{p},\boldsymbol{k})\, A_l^* A_p^*\}. \tag{3.2}$$

Here we have followed the notation given in (2.26) and also define

$$h(\boldsymbol{k},\boldsymbol{l},\boldsymbol{m}) = \left(\frac{V_l V_m}{V_k}\right)^{\frac{1}{2}}\left(\boldsymbol{l}\cdot\boldsymbol{m} + lm\right) + \left(\frac{V_k V_l}{V_m}\right)^{\frac{1}{2}}\left(\boldsymbol{k}\cdot\boldsymbol{l} + kl\right) + \left(\frac{V_k V_m}{V_l}\right)^{\frac{1}{2}}(\boldsymbol{k}\cdot\boldsymbol{m} + km). \tag{3.3}$$

To develop the spectral transport equation we require an ensemble average over the quasi-linear variables in the domain of triad resonances. In analogy to (2.15) and (2.16) we introduce the quasi-linear spectrum $\hat{\Psi}(\boldsymbol{k})$ and the quasi-linear action density

$$\hat{F}(\boldsymbol{k}) = \frac{\langle I_k\rangle_{\mathrm{c}}}{(2\pi)^2} = V_k \hat{\Psi}(\boldsymbol{k}), \tag{3.4}$$

where the ensemble average is carried out over amplitudes in the restricted capillary resonance domain. Applying the decomposition (1.3) to the quasi-linear waves, we set

$$\hat{F}(\boldsymbol{k}) = \hat{F}_{\mathrm{D}}(\boldsymbol{k}) + \hat{F}_{\mathrm{c}}(\boldsymbol{k}), \quad \hat{\Psi}(\boldsymbol{k}) = \hat{\Psi}_{\mathrm{D}}(\boldsymbol{k}) + \hat{\Psi}_{\mathrm{c}}(\boldsymbol{k}). \tag{3.5}$$

The derivation of the spectral transport equation for the quasi-linear action density follows that of Valenzuela & Laing (1972) and van Gastel (1987*a*) for the physical action density. We shall therefore not repeat this development here, but refer the reader to one of these papers. The resulting equation is

$$\partial \hat{F}_{\mathrm{c}}(\boldsymbol{k})/\partial t = \hat{S}_{\mathrm{t}}(\boldsymbol{k}), \tag{3.6}$$

where

$$\hat{S}_t(\boldsymbol{k}) = \frac{\pi}{8}\int d\boldsymbol{l}\, d\boldsymbol{p}\, \frac{\Gamma^2(\boldsymbol{k},\boldsymbol{l},\boldsymbol{p})}{V_k V_l V_p}\,\delta(\omega_k-\omega_l-\omega_p)\,\delta(\boldsymbol{k}-\boldsymbol{l}-\boldsymbol{p})$$
$$\times[\hat{F}(\boldsymbol{l})\,\hat{F}(\boldsymbol{p})-\hat{F}(\boldsymbol{k})(\hat{F}(\boldsymbol{l})+\hat{F}(\boldsymbol{p}))]$$
$$+\frac{\pi}{4}\int d\boldsymbol{l}\, d\boldsymbol{p}\, \frac{\Gamma^2(\boldsymbol{l},\boldsymbol{k},\boldsymbol{p})}{V_k V_l V_p}\,\delta(\omega_k-\omega_l+\omega_p)\,\delta(\boldsymbol{k}-\boldsymbol{l}+\boldsymbol{p})$$
$$\times[\hat{F}(\boldsymbol{l})\,\hat{F}(\boldsymbol{p})+\hat{F}(\boldsymbol{k})(\hat{F}(\boldsymbol{l})-\hat{F}(\boldsymbol{p}))]. \tag{3.7}$$

The arguments leading to (1.5) have here been applied to the quasi-linear wave system. Because of the specific form of (2.44), we have replaced the Ω by the linear wave ω in the δ-functions of (3.7).

The equilibrium condition for the direct-generation model is

$$\hat{S}_t(\boldsymbol{k}) = 0. \tag{3.8}$$

The dimensionless spectrum $\hat{B}(\boldsymbol{k})$ of quasi-linear waves is defined (compare (2.45)) by the equation

$$\hat{F}(\boldsymbol{k}) = V_k \alpha_D \hat{B}(\boldsymbol{k})/k^4. \tag{3.9}$$

Consistent with the decomposition (3.5), we separate $\hat{B}$ into two parts:

$$\hat{B} = \hat{B}_D + \hat{B}_c. \tag{3.10}$$

Since the quantities $\hat{B}$ are relatively slowly varying with wavenumber, they are useful for analysing (3.6) and (3.7).

It is seen that two kinds of triad resonances contribute to (3.7)

$$\boldsymbol{k} = \boldsymbol{l}+\boldsymbol{p}, \quad \omega_k = \omega_l+\omega_p, \text{ sum resonances}, \tag{3.11}$$

and

$$\boldsymbol{k} = \boldsymbol{l}-\boldsymbol{p}, \quad \omega_k = \omega_l-\omega_p, \text{ difference resonances}. \tag{3.12}$$

In fact, these differ only by a relabelling of wavenumbers. Because we are allowing no waves of wavelength less than 0.6 cm, the triad resonances are restricted to the wave domain D_R, which is

$$0.6 < \lambda < 10 \text{ cm}. \tag{3.13}$$

All three waves must lie in the domain (3.13) if a resonance is to occur. This observation permits us to now give a precise definition of H_{1R}, (2.34), and R, (2.43). The three wavenumbers occurring in the terms of H_{1R} all lie in the domain D_R. At least one of the three wavenumbers in the terms of R does not lie in D_R. It is to be noted that the sum resonance provides the principal contribution to our calculations.

The smallest value of k for which the sum resonance occurs is

$$k_m = (2g/\tau)^{\frac{1}{2}} = 511 \text{ m}^{-1}, \tag{3.14}$$

corresponding to a wavelength $\lambda_m = 1.23$ cm.

Because of the observational basis for the D-P spectrum in the wind regime, as determined from (1.4), it seems appropriate to set $S_t(\boldsymbol{k}) = 0$ for $k > k_m$. The contribution from the dominant sum resonance vanishes anyway in this domain, while that from the difference resonance is assumed to be absorbed in the phenomenology of D-P.

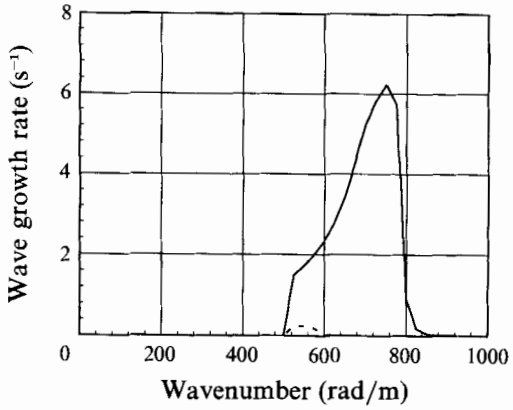

FIGURE 3. The growth rate a of (3.15) for downwind waves is shown as a function of wavenumber for 4 (dashed curve) and 6 m/s (solid curve) wind speeds.

On re-expressing (3.6) and (3.7) in terms of the dimensionless spectrum $\hat{B}$, we see that (3.6) is of the form

$$\frac{\partial \hat{B}_c(\boldsymbol{k})}{\partial t} = a(\boldsymbol{k}) - b(\boldsymbol{k})\,\hat{B}(\boldsymbol{k}). \tag{3.15}$$

The quantity $a(\boldsymbol{k})$ here represents the source term for generation of waves of wavenumber $\boldsymbol{k}$ and $b(\boldsymbol{k})$ represents a decay rate for these waves. The physical mechanisms which b describes represent flow of wave action to other wavenumbers – not true dissipation as represented by S_v in (1.1).

To evaluate $a(\boldsymbol{k})$ and $b(\boldsymbol{k})$ in (3.15) it appears to be a satisfactory approximation to replace the spectral amplitudes $\hat{B}$ in the integrands by the D-P spectrum B_D.

Because of the strong decrease of $\hat{F}$ with increasing wavenumber, we expect the integrals in (3.7) to be heavily weighted by the smallest wavenumbers consistent with the resonance conditions. Beyond the 'wind' regime of figure 1 the action amplitudes are relatively small. Within the wind regime CHSW did not find a significant difference between $\hat{F}$ and F, so we take

$$\hat{B}_D = B_D. \tag{3.16}$$

For the difference resonance integral in (3.7) we shall drop those terms involving $\hat{F}(\boldsymbol{l})$, since here $l > k, p$ and thus $\hat{F}(\boldsymbol{l})$ is relatively small. Therefore, we can write

$$a = a_s, \quad b = b_s + b_d, \tag{3.17}$$

where the subscript s refers to the sum resonance and d refers to the difference resonance in (3.7), and evaluation by numerical integration is straightforward. Analytic integration was performed in the neighbourhood of certain integrable singularities.

In figure 3 we show the growth rate $a(\boldsymbol{k})$ for downwind waves and wind speeds of 4 and 6 m/s. It is instructive to compare the damping coefficient $b(\boldsymbol{k})$ in (3.15) with that due to viscosity. The viscous damping term S_v in (1.1) is of the form

$$S_v = -\beta(k)\,F(\boldsymbol{k}), \quad \beta = 4\nu k^2, \tag{3.18}$$

where ν is the kinematic viscosity, which we take as

$$\nu = 1.1 \times 10^{-6}\ \mathrm{m^2/s}. \tag{3.19}$$

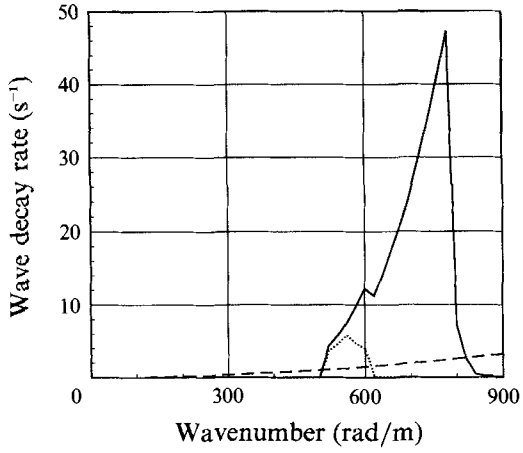

FIGURE 4. The decay rate b of (3.15) is compared with the viscous damping coefficient (3.17) (dashed curve). The wind speed for the solid curve is 6 m/s and for the dotted curve is 4 m/s. The waves are directed downwind.

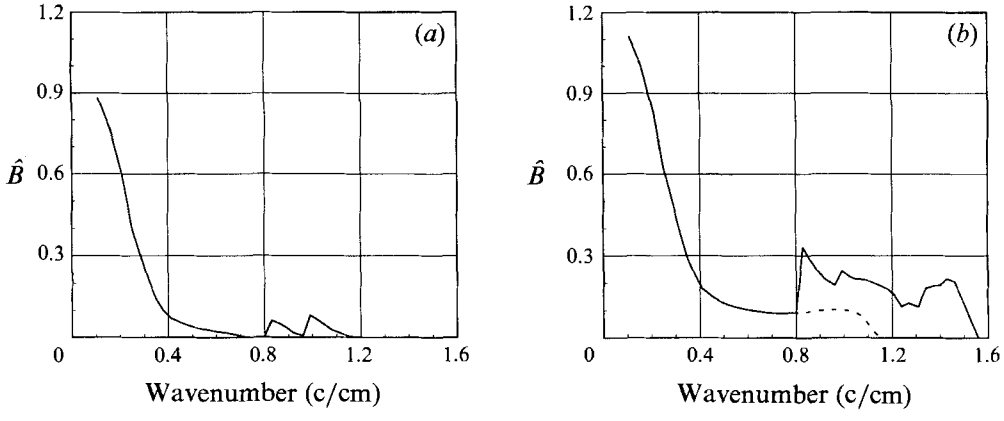

FIGURE 5. The quasilinear spectrum $\hat{B}(\boldsymbol{k})$ obtained using (3.20) is shown in the downwind direction. (*a*) Wind speed of 4 m/s; for wavenumbers less than 0.8 c/cm, the spectrum is just the D-P spectrum B_{D}. (*b*) Wind speed of 6 m/s. The spectrum B_{D} is shown as the dashed curve.

In figure 4 we compare b with β for wind speeds of 4 and 6 m/s and downwind waves. It is seen that in the greater part of the dynamic range of figure 1 the viscous decay is relatively small. This provides justification for the 'direct generation' model (3.8). With the use of expression (3.15) this model gives the spectrum

$$\hat{B}_{\mathrm{c}}(\boldsymbol{k}) = [a(\boldsymbol{k}) - b(\boldsymbol{k})\, B_{\mathrm{D}}]/b(\boldsymbol{k}). \tag{3.20}$$

We do not, of course, consider (3.20) to be physically valid for such high wavenumbers that b is less than the viscous damping rate β.

Spectra obtained from (3.20) are shown in figures 5(*a*) and 5(*b*) for wind speeds of 4 and 6 m/s and downwind waves. For a wind speed $U = 4$ m/s we see that the wavenumber at which the D-P spectrum vanishes is less than k_{m}. At 6 m/s this wavenumber is greater than k_{m}. For comparison, in figure 5(*b*) we have shown as the dashed curve the quantity B_{D} in the range $k > k_{\mathrm{m}}$.

In § 1 we introduced a second model for calculating the dynamic wave spectrum. This

was called the modified D-P model and is specified by (1.6). Adapting this model to quasi-linear waves, we take

$$\frac{k^4 S_{\mathrm{v}}}{V_k} = -\beta(\boldsymbol{k})\,\alpha_{\mathrm{D}}\,\hat{B}, \quad \frac{k^4 S_{\mathrm{w}}}{V_k} = \beta_{\mathrm{w}}(\boldsymbol{k})\,\alpha_{\mathrm{D}}\,\hat{B}, \quad \frac{k^4 S_{\mathrm{DP}}}{V_k} = \omega_{\mathrm{k}}\,\alpha(\alpha_{\mathrm{D}}\,\hat{B})^{n+1}. \tag{3.21}$$

Here β_{w} is the wind generation growth rate in the form used by D-P and α and n are parameters introduced and defined by D-P. Using these quantities, the quasi-linear wave adaptation of (1.6) is

$$a+(\beta_{\mathrm{w}}-\beta-b)\,\hat{B}+\omega_k\,\alpha\alpha_{\mathrm{D}}^n\,\hat{B}^{n+1}=0. \tag{3.22}$$

The dynamic portion of the capillary spectrum may be calculated as

$$\hat{B}_{\mathrm{c}} = \hat{B}-B_{\mathrm{D}}. \tag{3.23}$$

In the D-P model the quantity $\hat{B}$ is calculated, as in (3.22), for $\boldsymbol{k}=\boldsymbol{k}_{\mathrm{w}}$ directed parallel to the wind. The model is extended to other wave angles by introducing a phenomenological spreading function $G(\theta,k)$. Here θ is the angle between $\boldsymbol{k}$ and the wind direction and $G(0,\boldsymbol{k})=1$. Then

$$\hat{B}(\boldsymbol{k}) = \hat{B}(\boldsymbol{k}_{\mathrm{w}})\,G(\theta,k). \tag{3.24}$$

The spreading function that we use here is that introduced by Donelan *et al.* (1985).

We shall discuss the spectra obtained from these equations in the next section after we have transformed back to physical variables.

4. The physical wave variables

We are now ready to carry out the transformation from quasi-linear to physical wave variables. Our discussion in doing this follows closely that of CHSW. In analogy to (2.11) and (2.27) we define the amplitude

$$A_k(\lambda) = (P_k(\lambda))^{\frac{1}{2}}\exp[-\mathrm{i}Q_k(\lambda)]. \tag{4.1}$$

Equations (2.29) imply that

$$A_k(0)=a_k, \quad A_k(1)=A_k. \tag{4.2}$$

On using (2.30), we obtain the relations

$$\frac{\partial A_k}{\partial\lambda} = \frac{A_k}{2P_k}\frac{\partial P_k}{\partial\lambda} - \mathrm{i}A_k\frac{\partial Q_k}{\partial\lambda} = -A_k\left[\frac{1}{2P_k}\frac{\partial R}{\partial Q_k}+\mathrm{i}\frac{\partial R}{\partial P_k}\right]. \tag{4.3}$$

We evaluate this using (2.43) and simplify the result by assuming that $k \gg 1$ (to be justified later):

$$\begin{aligned}\frac{\partial A_k}{\partial\lambda} \approx -\frac{\mathrm{i}}{2}\sum_l\left(\frac{V_k}{2A_0V_l}\right)^{\frac{1}{2}}[\hat{\boldsymbol{l}}\cdot(\boldsymbol{k}-\boldsymbol{l})\,A_{k-l}A_l/V_{|\boldsymbol{k}-\boldsymbol{l}|}^{\frac{1}{2}} \\ +\hat{\boldsymbol{l}}\cdot(\boldsymbol{k}+\boldsymbol{l})\,A_{k+l}A_l^*/V_{|\boldsymbol{k}+\boldsymbol{l}|}^{\frac{1}{2}}].\end{aligned} \tag{4.4}$$

These equations are conveniently transformed to $\boldsymbol{x}$-space with the definitions

$$\left.\begin{aligned}Z(\boldsymbol{x},t,\lambda) &= \sum_k A_k\,\mathrm{e}^{\mathrm{i}\boldsymbol{k}\cdot\boldsymbol{x}}/(2A_0V_k)^{\frac{1}{2}}, \\ \boldsymbol{D}(\boldsymbol{x},t,\lambda) &= -\sum_l\frac{\hat{\boldsymbol{l}}}{(2A_0V_l)^{\frac{1}{2}}}[A_l\mathrm{e}^{\mathrm{i}\boldsymbol{l}\cdot\boldsymbol{x}}+\mathrm{c.c.}].\end{aligned}\right\} \tag{4.5}$$

Here we restrict $\boldsymbol{k}$ to the domain D_{R} (relation (3.13)) and continue to assume that $l \ll k$. With the definitions (4.5), we can express (4.4) as

$$\frac{\partial Z}{\partial \lambda} = \boldsymbol{D} \cdot \nabla_x Z. \tag{4.6}$$

Because of our assumption that only long waves contribute to $\boldsymbol{D}$, we do not require as general a solution to (4.6) as was obtained in CHSW. As was discussed in the last section, we can set

$$\boldsymbol{D}(\boldsymbol{x}, t, \lambda) \approx \boldsymbol{D}(\boldsymbol{x}, t) = -\sum_l \frac{\hat{\boldsymbol{l}}}{2(2A_0 V_l)^{\frac{1}{2}}} [a_l \mathrm{e}^{\mathrm{i}\boldsymbol{l}\cdot\boldsymbol{x}} + \text{c.c.}], \tag{4.7}$$

independent of λ. Thus, $\boldsymbol{D}$ represents the horizontal displacement of a fluid element due to long-wave orbital currents. We can also assume on physical grounds that

$$|\partial D_i / \partial x_j| \ll 1 \quad (i,j = 1,2). \tag{4.8}$$

Using (4.8), we conclude from substitution into (4.6) that Z is a function of

$$\boldsymbol{u} = \boldsymbol{x} + (1-\lambda)\boldsymbol{D}, \tag{4.9}$$

but does not otherwise depend on λ.

A Fourier expansion of Z in the rectangular area A_0 will be of the form

$$Z(\boldsymbol{x}, t, \lambda) = \sum_{\boldsymbol{k}} \frac{b_{\boldsymbol{k}}}{(2A_0 V_k)^{\frac{1}{2}}} \mathrm{e}^{\mathrm{i}\boldsymbol{k}\cdot\boldsymbol{u}}, \tag{4.10}$$

where the $b_{\boldsymbol{k}}$ may depend on t, but not on λ. We can determine the amplitudes $\boldsymbol{b}_{\boldsymbol{k}}$ above by setting $\lambda = 1$ in (4.5) and (4.10). A comparison of the two expression shows that

$$b_{\boldsymbol{k}} = A_{\boldsymbol{k}}, \tag{4.11}$$

the quasi-linear wave amplitude. The physical vertical displacement of the water surface is then (see (2.8))

$$\zeta(\boldsymbol{x}, t) = \mathrm{i}[Z(\boldsymbol{x}, t, 0) - \text{c.c.}], \tag{4.12}$$

where

$$Z(\boldsymbol{x}, t, 0) = \sum_{\boldsymbol{k}} \frac{A_{\boldsymbol{k}}}{(2A_0 V_k)^{\frac{1}{2}}} \exp[\mathrm{i}\boldsymbol{k}\cdot(\boldsymbol{x} + \boldsymbol{D}(\boldsymbol{x}))]. \tag{4.13}$$

The displacement spectrum for the capillary domain is

$$\Psi_{\mathrm{c}}(\boldsymbol{k}) = \frac{2}{(2\pi)^2 A_0} \left\langle \left| \int \mathrm{d}\boldsymbol{x}\, \mathrm{e}^{-\mathrm{i}\boldsymbol{k}\cdot\boldsymbol{x}} Z(x, t, 0) \right|^2 \right\rangle. \tag{4.14}$$

Using (3.4), we can write this in the form

$$\Psi_{\mathrm{c}}(\boldsymbol{k}) = \frac{1}{(2\pi)^2 A_0} \int \mathrm{d}\boldsymbol{x}\, \mathrm{d}\boldsymbol{y} \int \mathrm{d}\boldsymbol{p}\, \mathrm{e}^{\mathrm{i}(\boldsymbol{y}-\boldsymbol{x})\cdot(\boldsymbol{k}-\boldsymbol{p})}\, \hat{\Psi}_{\mathrm{c}}(\boldsymbol{p}) \langle \mathrm{e}^{\mathrm{i}\boldsymbol{p}\cdot(\boldsymbol{D}(\boldsymbol{x})-\boldsymbol{D}(\boldsymbol{y}))} \rangle. \tag{4.15}$$

We are assuming the displacement $\boldsymbol{D}$ to be a Gaussian variable, so

$$\langle \exp[\mathrm{i}\boldsymbol{p}\cdot(\boldsymbol{D}(\boldsymbol{x}) - \boldsymbol{D}(\boldsymbol{y}))] \rangle = \exp[-p^2 G(\boldsymbol{r})], \tag{4.16}$$

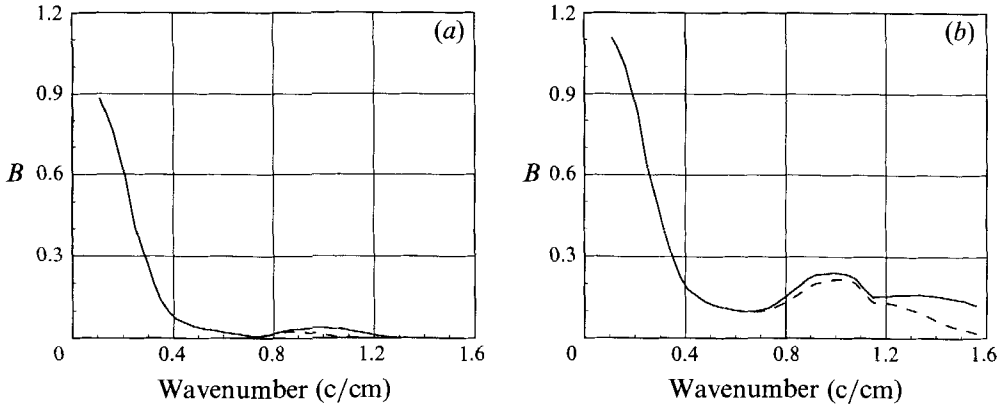

FIGURE 6. The dimensionless spectrum B, as obtained from (4.20), is shown for waves travelling downwind. The solid curve represents the direct-generation spectrum (obtained from (3.19)) and the dashed curve the modified D-P spectrum (obtained from (3.21)). (*a*) Wind speed of 4 m/s; the quasi-linear spectrum of figure 5(*a*) was used in (4.18) to obtain the solid curve. (*b*) Wind speed of 6 m/s. The spectrum of figure 5(*b*) was used in (4.18) to obtain the solid curve.

where $\boldsymbol{r} = \boldsymbol{x} - \boldsymbol{y}$ and

$$G(\boldsymbol{r}) = \int \mathrm{d}\boldsymbol{l} (\hat{\boldsymbol{p}} \cdot \hat{\boldsymbol{l}})^2 [1 - \cos(\boldsymbol{l} \cdot \boldsymbol{r})] \, \Psi(\boldsymbol{l}). \tag{4.17}$$

Finally,

$$\Psi_{\mathrm{c}}(\boldsymbol{k}) = \int \mathrm{d}\boldsymbol{p} \, I(\boldsymbol{k}, \boldsymbol{p}) \, \hat{\Psi}_{\mathrm{c}}(\boldsymbol{p}), \tag{4.18}$$

Here

$$I(\boldsymbol{k}, \boldsymbol{p}) = \frac{1}{(2\pi)^2} \int \mathrm{d}\boldsymbol{r} \, \mathrm{e}^{\mathrm{i}(\boldsymbol{p} - \boldsymbol{k}) \cdot \boldsymbol{r}} \exp[-p^2 G(\boldsymbol{r})]. \tag{4.19}$$

To evaluate I the spectrum of Donelan *et al.* (1985) was used. For reasons of numerical convenience, the integration in (4.17) was restricted to the domain $l < l_{\mathrm{c}} = 10\ \mathrm{m}^{-1}$ and an analytic model for I was constructed, based on numerical integration. (The effect of changing the cutoff l_{c} to $20\ \mathrm{m}^{-1}$ did not give more than a 7% change in (4.18)).

The complete surface wave spectrum is then

$$\Psi(\boldsymbol{k}) = \Psi_{\mathrm{D}}(\boldsymbol{k}) + \Psi_{\mathrm{c}}(\boldsymbol{k}). \tag{4.20}$$

The direct-generation spectrum is obtained using (3.19) in (4.18), while the modified D-P spectrum is given with the use of (3.21) in (4.18). We illustrate this in figure 6(*a*), where $B(\boldsymbol{k})$ is shown for a wind speed of 4 m/s and downwind waves. The solid curve represents the direct-generation spectrum, while the dashed curve corresponds to the modified D-P spectrum. As expected, because of the damping in (3.22), the modified D-P spectral levels are lower than those for the direct-generation model. The role of nonlinear straining is seen when figures 5(*a*) and 6(*a*) are compared.

In figure 6(*b*) we show the corresponding spectra for a wind speed of 6 m/s. Again, we see the effect of straining when figures 5(*b*) and 6(*b*) are compared.

The angular distribution of the dynamic wave slope spectrum about the angle θ between the wind direction and $\boldsymbol{k}$ is

$$\frac{\mathrm{d}\langle m^2 \rangle}{\mathrm{d}\theta} = \int \Psi_{\mathrm{c}}(\boldsymbol{k}) \, k^3 \, \mathrm{d}k, \tag{4.21}$$

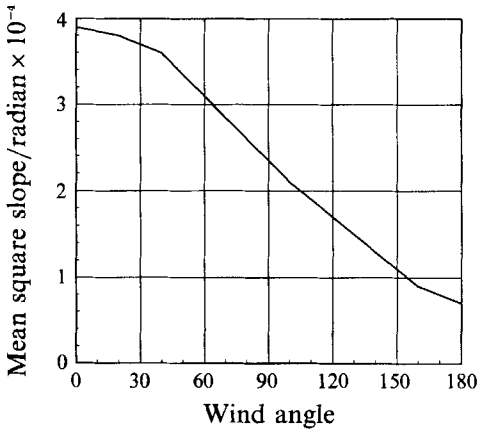

FIGURE 7. The angular distribution (4.21) of the mean-square slope/radian of the dynamic waves is shown as a function of the angle between wind and wave direction for a wind speed of 6 m/s.

where the direct-generation model is used. We illustrate (4.21) in figure 7 for a wind speed of 6 m/s.

5. Discussion

We have not addressed the delicate question of terminating the expansion (2.38). (We are not alone here; see, however, Milder 1990.) It would appear to be feasible to avoid the Hasselmann approximation (3.6), (3.7) by numerically integrating the set of equations (3.2). Defined only in the restricted domain D_R (see (3.13)) and being of second order in the wave amplitudes, these equations are much simpler than those investigated by West *et al.* (1987).

A further limitation on our work results from the need to match phenomenological models for the longer wavelengths to our theoretical calculations for the shortest waves. The lack of dissipation in the direct-generation model is a clear shortcoming. Again, we have had to use the parameters of the D-P model at higher wavenumbers than seems justified by the data from which it was deduced.

Recognizing these limitations on the quantitative aspects of our calculations, we now see how these compare with the observations of Jähne & Riemer (1990). First, to within a nominal factor of two or so our two models are not very different. Dissipation in the modified D-P model evidently reduces the spectrum levels, as is seen from figures 6(*a*) and 6(*b*).

At 4 m/s wind speed the direct model agrees rather well at 1 c/cm wavelength with the data of Jähne & Riemer (their figure 9*a*). The modified D-P model spectrum is about a factor of two below this. At 6 m/s wind speed and 1 c/cm wavenumber, the direct-generation model is a little high, but the modified D-P model is in fair agreement. The measured spectrum falls off above 1.4 c/cm, as does the modified D-P spectrum. The direct-generation spectrum does not do this, presumably due to the lack of dissipation in it. The minimum in our calculated spectra near the transition from wind to dynamic regimes is, if present, much less evident in the low-wind-speed data. The angular distribution shown in figure 7 is in fair agreement with that indicated by figures 9(*a–c*) of Jähne & Riemer.

The qualitative agreement between our calculations and the observations of Jähne & Riemer (1990) suggests that the dynamic generation mechanism used here is of

physical importance for the generation of the shortest capillary waves at low wind speeds. We have refrained from extending our calculations to higher wind speeds, for which wind-driven surface currents and wave breaking are expected to complicate the physics.

The work of K. M. W. was supported in part by ONR Contract N00014-80-C-0220.

REFERENCES

CASE, K. M. 1966 A general perturbation method for quantum mechanical problems. *Prog. Theor. Phys. Suppl.* Nos. 37, 38.

CHIRIKOV, B. V. 1977 A universal instability of many-dimensional oscillator systems. *Phys. Rep.* **52**, 264–379.

COX, C. S. 1958 Measurements of slopes of waves. *J. Mar. Res.* **16**, 199–225.

CREAMER, D., HENYEY, F., SCHULT, R. & WRIGHT, J. 1989 Improved linear representation of ocean surface waves. *J. Fluid Mech.* **205**, 135–161 (referred to herein as CHSW).

DONELAN, M., HAMILTON, J. & HUI, W. 1985 Directional spectra of wind-generated waves. *Phil. Trans. R. Soc. Lond* A **315**, 509–562.

DONELAN, M. & PIERSON, W. 1987 Radar scattering and equilibrium ranges in wind-generated waves with applications to scatterometry. *J. Geophys. Res.* **92**, 4971–5030 (referred to herein as D-P).

GASTEL, K. VAN 1987*a* Nonlinear interactions of gravity–capillary waves: Lagrangian theory and effects on the spectrum. *J. Fluid Mech.* **182**, 499–523.

GASTEL, K. VAN 1987*b* Imaging by X-Band radar of subsurface features: A nonlinear phenomena. *J. Geophys. Res.* **92**, 11857–11866.

GOLDSTEIN, H. 1959 *Classical Mechanics*. Addison-Wesley.

HASSELMANN, K. 1968 Weak-interaction theory of ocean waves. In *Basic Developments in Fluid Mechanics* (ed M. Holt), pp. 117–182. Academic.

HENYEY, F., CREAMER, D., DYSTHE, K., SCHULT, R. & WRIGHT, J. 1988 The energy and action of small waves riding on large waves. *J. Fluid Mech.* **189**, 443–462.

HOLLIDAY, D. 1977 On nonlinear interactions in a spectrum of inviscid gravity–capillary surface waves. *J. Fluid Mech.* **83**, 737–749.

HUGHES, B. A. 1978 The effects of internal waves on surface waves: 2. Theoretical analysis. *J. Geophys. Res.* **83**, 455–465.

JÄHNE, B. & RIEMER, K. 1990 Two-dimensional wave number spectra of small scale water surface waves. *J. Geophys. Res.* **95**, 11531–11546.

LONGUET-HIGGINS, M. S. 1962 The generation of capillary waves by steep gravity waves. *J. Fluid Mech.* **16**, 138–159.

MEISS, J. & WATSON, K. 1978 Discussion of some weakly nonlinear systems in continuum mechanics. In *Topics in Nonlinear Dynamics* (ed. S. Jorna) AIP Conf. Proc. 46, pp. 296–323.

MILDER, D. M. 1990 The effects of truncation on surface-wave Hamiltonians. *J. Fluid Mech.* **217**, 249–262.

MILES, J. W. 1977 On Hamilton's principle for surface waves. *J. Fluid Mech.* **83**, 153–164.

MILLER, S., SHEMDIN, O. & LONGUET-HIGGINS, M. 1992 Laboratory measurements of modulation of short-wave slopes by long surface waves. *J. Fluid Mech.* **233**, 389–404.

PHILLIPS, O. M. 1985 Spectral and statistical properties of the equilibrium range in wind-generated gravity waves. *J. Fluid Mech.* **156**, 505–531.

VALENZUELA, G. & LAING, M. 1972 Nonlinear energy transfer in gravity–capillary wave spectra with applications. *J. Fluid Mech.* **54**, 507–520.

WATSON, K. & WEST, B. 1975 A transport equation description of nonlinear ocean surface wave interactions. *J. Fluid Mech.* **70**, 815–826.

WEST, B., BRUECKNER, K., JANDA, R., MILDER, D. & MILTON, R. 1987 A new numerical method for surface hydrodynamics. *J. Geophys. Res.* **92**, 11803–11824.